



OPEN

## Spectroscopic ellipsometry modelling of Cr<sup>+</sup> implanted copper oxide thin films

K. Ungeheuer<sup>1✉</sup>, K. W. Marszalek<sup>1</sup>, M. Mitura-Nowak<sup>2</sup> & A. Rydysz<sup>1</sup>

In this paper, we present modelling of spectroscopic ellipsometry data. The measured samples are thin films of copper oxides modified with the ion implantation method. The samples were prepared using reactive magnetron sputtering. Thin films of CuO and Cu<sub>4</sub>O<sub>3</sub> were deposited and subjected to Cr ion implantation with an energy of 15 keV and a dose of  $5 \times 10^{16}$  ions/cm<sup>2</sup>. The decrease in crystallinity of the thin film as a result of the implantation was inspected with X-ray diffraction measurements. The implantation of Cr<sup>+</sup> ions was simulated using the Stopping and Range of Ions in Matter software by Ziegler and Biersack. Ion beam energy of 15 keV was simulated to estimate the distribution of Cr ions in the copper oxides thin films. Optical parameters, such as refractive index, extinction coefficient, and absorption coefficient of the thin films, were investigated with spectroscopic ellipsometry. Multilayered models based on Tauc–Lorentz oscillators were developed for both oxides. Analysis of the optical properties showed that the ion implantation with Cr decreased the absorption of copper oxides thin films and the modelling proved that the material properties of top layers changed the most.

Copper oxides are known semiconductors with a high absorption coefficient. Their optical and photocatalytic properties bring great interest among researchers<sup>1–3</sup>. Although most researchers focus on studies of cupric (CuO) and cuprous (Cu<sub>2</sub>O) oxides, where paramelaconite (Cu<sub>4</sub>O<sub>3</sub>) is not investigated that much, where a good example is that the first application of Cu<sub>4</sub>O<sub>3</sub> in a solar cell system was published in 2012, while copper oxide Cu<sub>2</sub>O was one of the first photovoltaic materials<sup>4</sup>. Possible applications of copper oxides are in photovoltaics<sup>3,5</sup>, sensors<sup>6,7</sup>, and photocatalysis<sup>8,9</sup>. However, the performance of the material is lower than expected theoretically. For example, copper oxides as photovoltaic absorbers in thin-film solar cells should give energy conversion efficiency of 20% (Cu<sub>2</sub>O) or even 30% (CuO), based on the Shockley–Quisser limit and the value of the energy band gap of the oxides. Meanwhile, the best performances of solar cells with copper oxide as an absorber cannot reach even 10% efficiency<sup>10,11</sup>. Modifications are crucial to improve properties of copper oxides thin films and achieve better performance in photovoltaics<sup>12</sup> and other applications.

Here we report research with copper oxides modification using the ion implantation method. We chose for our experiment one of well studied oxides—CuO, and Cu<sub>4</sub>O<sub>3</sub> as the reports on this material are few. We chose Cr as dopant, as it is a transition metal and can improve the electrical properties of copper oxides<sup>13</sup>. In other works, the researchers used Na<sup>14</sup>, Co<sup>15</sup>, Ag, Au, Cr, Pd, Pt, Sb, Si<sup>16</sup>, and Ni<sup>17</sup> as dopants to modify the properties of copper oxides. Furthermore, Cr has been proved to enhance the sensing performance of copper oxides<sup>18</sup> and increase the V<sub>OC</sub> and I<sub>SC</sub> of a CuO:Cr/p-Si p–n junction, which is favourable in solar cell applications<sup>19</sup>.

Ion implantation is a method of material doping widely used in the semiconductor industry<sup>20,21</sup>. This technique enables us to input dopant atoms to the required depth of the material. The process also induces damage and even amorphization of the target film, thus annealing and recrystallisation of a semiconductor is necessary to achieve desired electrical properties. Ion implantation was also used as a modification method for copper oxides, for example, with N ions to introduce a phase change<sup>22</sup>, or the tune electrical and optical properties<sup>23</sup>. CuO nanowires were modified with Fe and N ion irradiation by Sisman et al.<sup>24</sup> where energy of 60 and 100 keV was used, with a fluence of  $1 \times 10^{13}$  and  $2.5 \times 10^{16}$  cm<sup>-2</sup>. The thin film consisting of nanowires was about 1 μm thick. The electrical and sensing properties were improved, though the X-ray diffraction measurements did not allow to see any structural changes caused by implantation, only using the X-ray photoelectron spectroscopy they could state phase changes after implantation to Cu<sub>2</sub>O and Cu(OH)<sub>2</sub>. Another utilization of ion implantation was performed by Shi et al.<sup>25</sup>, who used argon ions to introduce defects into CuO to study the magnetic properties of the material. High energy 2 MeV Ar ions with doses of  $1 \times 10^{15}$  and  $5 \times 10^{15}$  cm<sup>-2</sup> produced an increased amount of

<sup>1</sup>Faculty of Computer Science, Electronics and Telecommunications, AGH University of Krakow, 30 Mickiewiczza Ave., 30-059 Krakow, Poland. <sup>2</sup>Henryk Niewodniczanski Institute of Nuclear Physics, 152 Walerego Eljasza Radzikowskiego Str., 31-342 Krakow, Poland. ✉email: ungeheue@agh.edu.pl

the Cu vacancies and cause a phase change of CuO into Cu<sub>2</sub>O. Yadav et al.<sup>26</sup> implanted CuO thin films of 220 nm thickness with Ag ions of 30 keV energy and doses between  $1 \times 10^{14}$  and  $1 \times 10^{16}$  cm<sup>-2</sup>. They found that with higher dose the crystallinity of material decreased, and they also noticed a phase change—into Cu<sub>2</sub>O and even Cu for the highest implantation dose. Atomic force microscopy showed an increase in roughness after implantation. The energy band gap of CuO determined with diffused reflectance spectroscopy was reduced with implantation. However, no reports have been published on the use of ion implantation to modify Cu<sub>4</sub>O<sub>3</sub> thin films.

To study the influence of implantation, we characterised the structural and optical properties of the thin films with X-ray diffraction (XRD) and spectroscopic ellipsometry (SE), respectively. To analyse the data obtained with the SE method, a model of material dielectric function is required. Here we designed a model based on the Tauc–Lorentz oscillators and information on energy transitions that occur in copper oxides. In a review of copper oxides Meyer et al.<sup>4</sup> studied the dielectric function of these materials, and provided  $\epsilon_2$  transition energies. The models used in this work were created on the basis of that information.

We additionally performed simulations to find how deep ions induce changes in the material, for this purpose we used software of Stopping and Range of Ions in Matter (SRIM)<sup>27</sup>. The calculation gives many items of information as output, enabling us to study how ions interact with the target. The calculations of this program are based on two main effects, the electrical and nuclear stopping powers, which correspond to the interaction of the implanted ions with the bound electrons and nuclei of the target atoms, respectively. The simulation assumes that the material is amorphous and therefore channelling effects are not considered. The software requires as input parameters the composition of the target material, its thickness and density, as well as information about the implantation beam: type of ion, energy, and angle of incidence. The package returns information about the range and straggling of implanted atoms, the damage caused by recoil cascades, energy absorption, and ionisation of target atoms.

## Material and methods

### Film deposition

The cupric oxide and paramelaconite thin films were deposited with the DC reactive magnetron sputtering method. The substrate used was monocrystalline silicon to perform characterisation of deposited films with X-ray diffraction and spectroscopic ellipsometry. Before deposition, the substrates were cleaned with warm water and soap, and then submerged in isopropanol for 20 min of an ultrasonic bath. For deposition of thin films we used a 99.95% purity copper target from Kurt J. Lesker; the distance between the substrates and the target was 5 cm. During the sputtering process, the substrates were heated to 150 °C. Before the deposition itself, a pre-sputtering process was performed, with the aim of clearing the target and creating ions needed for the sputtering process. The pre-sputtering lasted for 10 min in Ar and then for 20 min in working gas. For CuO deposition, the working pressure was 2.00 Pa and the atmosphere consisted of only O<sub>2</sub> with gas flow set at 30 sccm. For Cu<sub>4</sub>O<sub>3</sub> deposition, the working pressure was 1.51 Pa and the gas flow was set at 27 sccm of O<sub>2</sub> and 3 sccm of Ar. CuO samples were deposited with thicknesses of 30 nm, 55 nm, and 130 nm. Cu<sub>4</sub>O<sub>3</sub> films were deposited with thicknesses of 35 nm, 55 nm, and 115 nm.

### Characterisation

The samples were characterised with XRD and SE to study their structural and optical properties. We used the PANalytical X'Pert PRO diffractometer, with a Cu anode (0.154 nm radiation wavelength) for diffraction measurements. Ellipsometric measurements were performed with J.A. Woollam M 2000 ellipsometer. The thickness of thin films was measured with a Talystep profilometer.

### Ion implantation

Thin film samples were subjected to ion implantation with Cr ions at the Henryk Niewodniczanski Institute of Nuclear Physics in Krakow. The ion implantation equipment features a modified Bernas-type source of ions and electromagnets that precisely select the ions with desired energy and mass. As a source of Cr ions we used anhydrous chromium trichloride. The energy and dose of implanted ions were 15 keV and  $5 \times 10^{16}$  ion/cm<sup>2</sup>. The dose of ions was controlled by the time that a moving sample holder spent in front of the ion beam.

The implantation of Cr ions into copper oxides was simulated with the Stopping and Range of Ions in Matter software. For visualization of recoils 1000 ions were simulated, for other results 30,000 ions were simulated.

## Results and discussion

### Implantation simulations

SRIM simulations can provide information about the interaction of implanted ions and target atoms. Basic information is the distribution of implanted atoms, which depends on their energy, and the density and composition of the target. Therefore, for each copper oxide, the distribution of Cr ions will be different. The distribution of ions, and therefore their range, for CuO and Cu<sub>4</sub>O<sub>3</sub> implanted with 15 keV energy Cr ions are presented in Fig. 1a. The oxides CuO and Cu<sub>4</sub>O<sub>3</sub> have density of 6.315 g/cm<sup>3</sup> and 5.84 g/cm<sup>3</sup>, respectively. The difference in the ion range is not large, the composition of the oxides plays an important role here, Cu<sub>4</sub>O<sub>3</sub> has a higher ratio of Cu with respect to O than CuO, and the two elements have different displacement energies, which is the main cause of the difference in the ion depth distribution. Ionisation is in a greater share caused by recoils than ions, as presented in Fig. 1b. Cu<sub>4</sub>O<sub>3</sub> becomes more ionised than CuO when implanted with the same energy and dose of ions. The energy introduced by Cr ions can be absorbed by O or Cu atoms (Fig. 1d,e). In the case of Cu<sub>4</sub>O<sub>3</sub>, the Cu atoms absorb more energy than the O atoms (Fig. 1b), for CuO the absorption share is inverted (Fig. 1a), this is caused by differences in oxides composition. Energy absorption occurs mainly near the surface of the

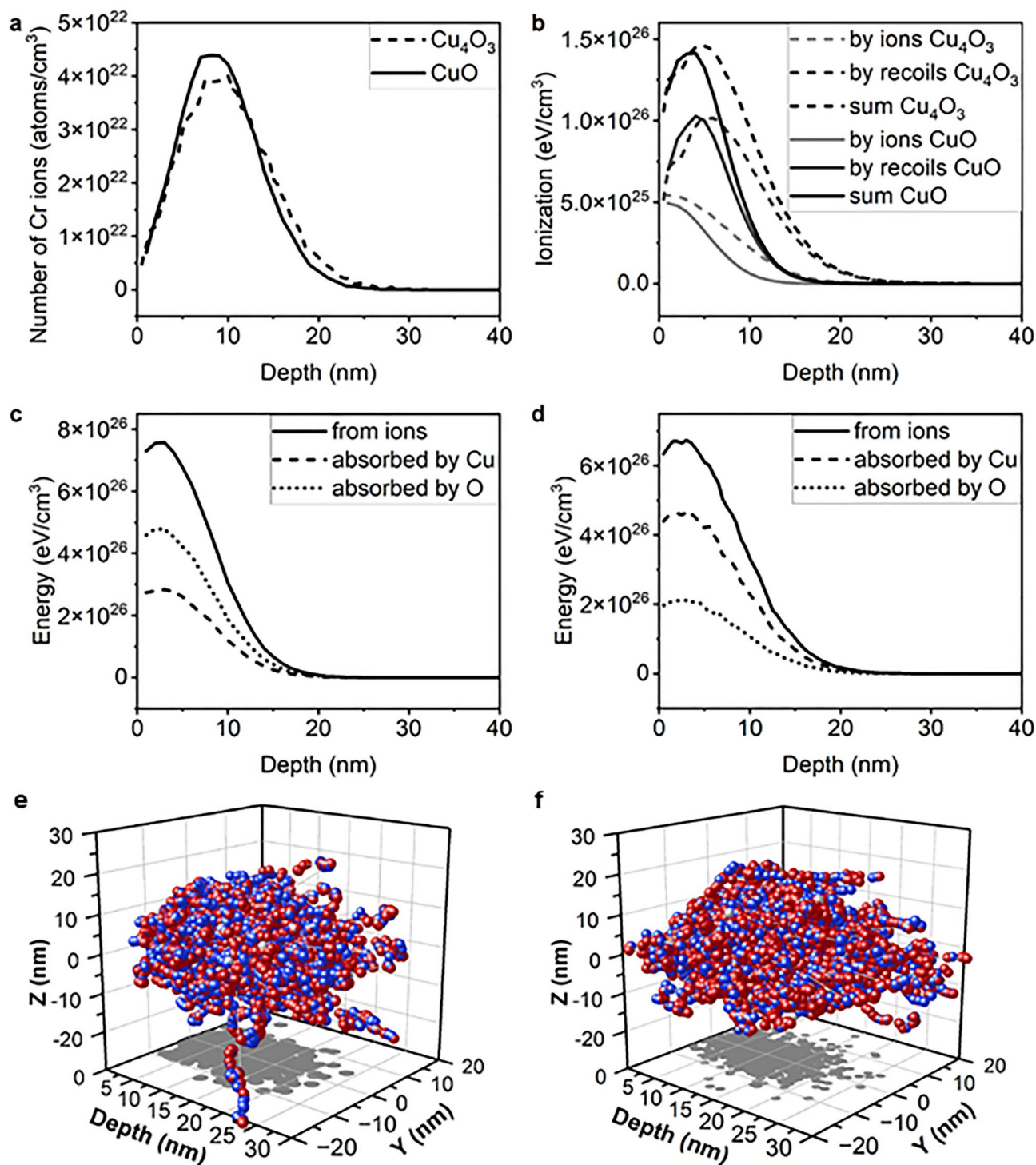


**Figure 1.** (a) Depth distribution of Cr ions implanted into copper oxides with energy of 15 keV and dose  $5 \times 10^{16} \text{ cm}^{-2}$ , (b) ionization of target atoms caused by ions and recoils, (c) energy brought by ions and its absorption by Cu and O atoms in implanted CuO and (d)  $\text{Cu}_4\text{O}_3$ , (e) recoil cascades for implantation of CuO (the balls represent atoms: grey—Cr ions, red—Cu, blue—O; an arrow indicates the beam incidence point; on XY plane a grey projection of Cr ions positions is presented) (f) recoil cascades for implantation of  $\text{Cu}_4\text{O}_3$ .

target and decreases in depth. The increase in the relative amount of the Cu atoms to the O atoms is responsible for a larger ionisation depth in  $\text{Cu}_4\text{O}_3$  oxide.

The SRIM package allows us to illustrate the recoil cascades and see how much more damage is spread by the recoils than just ions, also in the lateral direction to the beam. The simulation was carried out for ions with a  $0^\circ$  angle of incidence, where the beam enters the target at a single point. To calculate the data in Fig. 1a–d, 30,000 ions were simulated, while for the graphical presentation in Fig. 1e,f only 1000 ions were simulated. Each grey

ball represents a Cr ion, and red and blue balls represent copper and oxygen atoms, respectively. An energised ion knocks the target atoms of their positions, and if an atom has enough energy, it knocks another one, creating recoil cascades. This effect is more profound in the case of  $\text{Cu}_4\text{O}_3$ . The trajectories of 1000 simulated ions extend to a greater extent in directions perpendicular to the beam for  $\text{Cu}_4\text{O}_3$  (Fig. 1f) than CuO (Fig. 1e). It is important to emphasize that the results presented in Fig. 1e,f show the effect of only 1000 ions that enter the material at a single point (it is impossible to make graphical visualisations for larger amount of ions), while the real implantation experiment is subjected to the entire surface of the sample and the number of ions is drastically larger with a dose of  $5 \times 10^{16} \text{ cm}^{-2}$ .

### Structural properties—XRD

XRD measurements were performed to study how implantation changed the phase composition and crystallinity of the thin film copper oxides, as well as to confirm if the correct oxide was deposited. More detailed analysis, including the calculation of lattice strain and crystallite size, of Cr-implanted CuO thin films can be found in<sup>28</sup> (Fig. 2a). In Fig. 2a diffractograms of samples of 30 nm, 55 nm, and 130 nm are presented, all of them show clear CuO peaks (based on JPCDS card #01-080-0076). In the case of a 30 nm layer, the implantation completely amorphized the material, there are no visible peaks after implantation. The 55 nm sample after implantation shows peaks from Cu (JPCDS card #00-001-1242) and Si (JPCDS card #00-001-0787), while no clear peaks from CuO are visible. The thicker sample still shows CuO peaks after implantation. The ions implanted in the material lose their energy via excitation of target's electrons or collisions with nuclei. For energies in the range of keV, the nuclear stopping is predominant<sup>26</sup>. Collisions with target atoms cause them to move from their positions in the crystal lattice, the crystal structure is damaged and can be amorphized with enough implanted ions<sup>21</sup>. A portion of the target atoms can also be sputtered from the target, which could also be a reason for the absence of a signal from the implanted 30 nm sample. From this information, we can consider that the ions influence the crystal structure drastically up to 55 nm in depth, but a thicker layer is not damaged and still retains its crystal structure beyond the range of ion implantation. No Cr compounds were identified using the XRD method; one explanation is that no crystalline structures were formed by Cr, and another is that their amount was too little to be detected with this method.

The thinnest  $\text{Cu}_4\text{O}_3$  sample shows a peak coming from  $\text{Cu}_2\text{O}$  (JPCDS card #01-074-1230), indicating that deposition was not completely successful (Fig. 2b). For thicker samples, 115 nm and 55 nm, the film consists only of  $\text{Cu}_4\text{O}_3$  with peaks visible: (200), (202) and (404), (220)—JPCDS card #00-0491-830. After implantation, Cu peaks are visible (JPCDS card #00-001-1242). In the case of 55 nm sample, the crystal structure was deteriorated to such degree that the paramelaconite peaks are barely visible. The thin film was damaged by implantation. The thinnest sample is the most damaged as the ions and recoils influenced its entire thickness, and according to the simulation results, the range of recoil is about 30 nm. The 55 nm sample is heavily damaged as the recoils reach further in depth of material, and influence most of the sample. Therefore, to study optical properties with SE we chose only  $\text{Cu}_4\text{O}_3$  with a thickness of 115 nm.

For samples with thickness higher than 100 nm, the implantation had a more profound effect on  $\text{Cu}_4\text{O}_3$  than CuO. This corresponds to the results of the SRIM simulations where the ionisation and impact on target atoms are greater for  $\text{Cu}_4\text{O}_3$  (Fig. 1). In case of thinner samples, CuO crystal structure was more damaged, and for the thinnest sample no crystalline material was detected, this observation may be caused by difference in thickness between the samples CuO and  $\text{Cu}_4\text{O}_3$  samples ( $\text{Cu}_4\text{O}_3$  is slightly thicker).

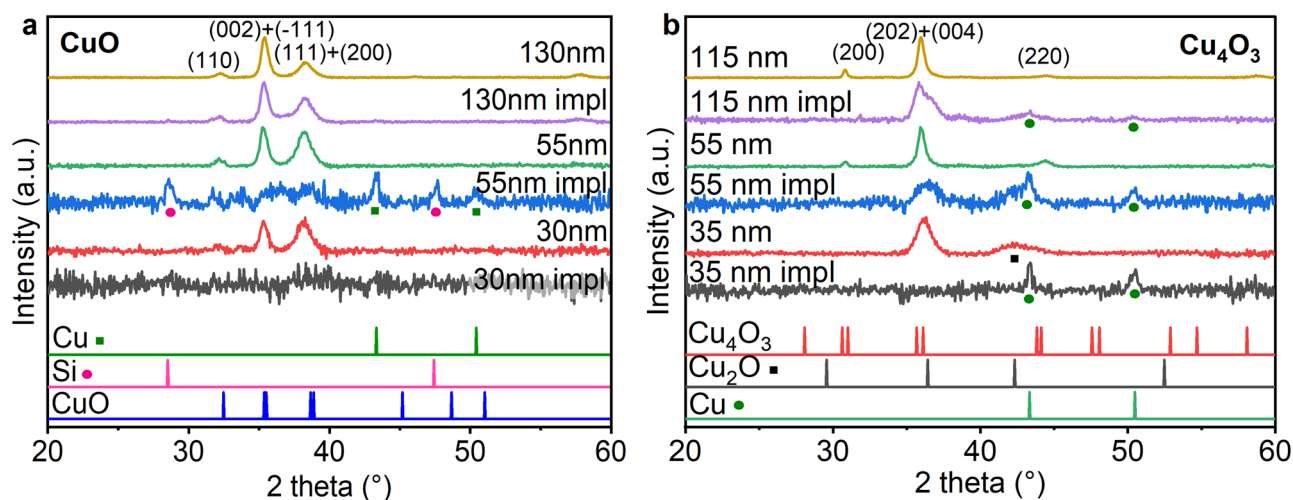


**Figure 2.** Diffractograms of thin films before and after implantation with Cr ions (a) CuO, (b)  $\text{Cu}_4\text{O}_3$ ; peaks for CuO and  $\text{Cu}_4\text{O}_3$  are designated.

### Optical properties—SE

Spectroscopic ellipsometry is a method that is used to study thin film samples, especially. In this technique, a polarised light beam is directed onto the sample and after reflection gets into the detector. The change in light polarisation is the result of SE measurement and is expressed as two parameters: Psi and Delta, which give information on the amplitude and phase changes, respectively. The measured data along with the fitted values are presented in Fig. 3a,b for the non-implanted and implanted Cu<sub>4</sub>O<sub>3</sub> samples.

To analyse the data, an optical model of the desired material must be used. Here, we establish models for CuO and Cu<sub>4</sub>O<sub>3</sub> based on information about energy transitions from<sup>4</sup> which is presented in Table 1 together with fitted values of the oscillators' energy positions  $E_0$ . We used Tauc–Lorentz oscillators to model each energy transition and multiple oscillators to model the dielectric function. The T-L oscillator is expressed as:

$$\begin{aligned}\varepsilon_{T-L}(E) &= \varepsilon_1 - i\varepsilon_2 \\ \varepsilon_2 &= \left[ \frac{AmpE_0Br(E - E_g)^2}{(E^2 - E_0^2)^2 + Br^2E^2} \cdot \frac{1}{E} \right], E > E_g \\ \varepsilon_2 &= 0, E \leq E_g \\ \varepsilon_1 &= \frac{2}{\pi} P \int_{E_g}^{\infty} \frac{\xi' \varepsilon_2(\xi)}{\xi^2 - E^2} d\xi\end{aligned}\quad (1)$$

where  $\varepsilon_1$ —real part of dielectric function,  $\varepsilon_2$ —imaginary part of dielectric function,  $E_g$ —energy band gap,  $E$ —photon energy,  $E_0$ —peak central energy, Amp—amplitude, Br—broadening, P—Cauchy principal value.

The model for CuO consists of a Si substrate, three layers of CuO, and a roughness layer. Each CuO layer consists of 4 Tauc–Lorentz oscillators. The roughness layer is a volume sum of 50% void and 50% of the layer

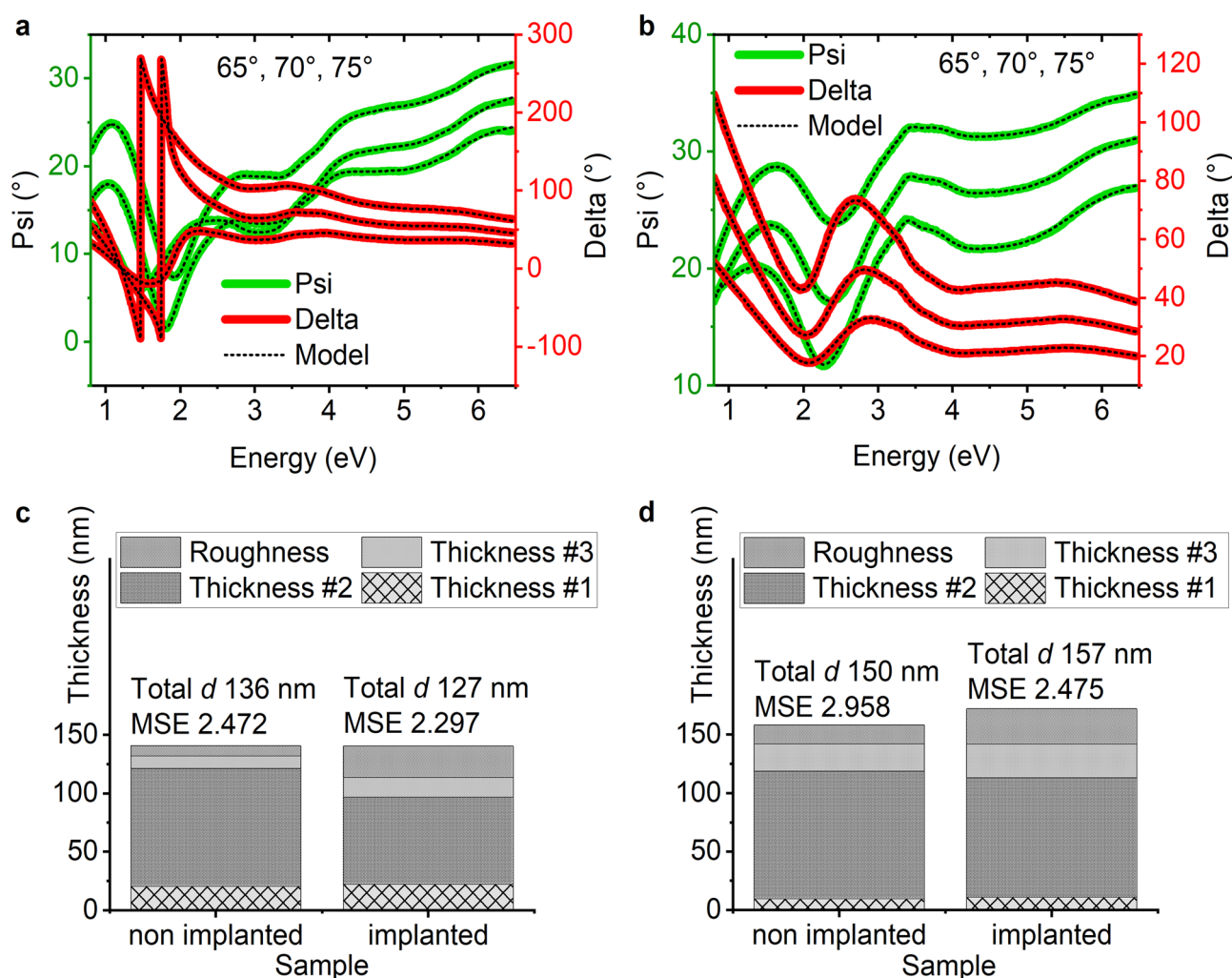


**Figure 3.** SE measured Psi and Delta data and fitted model values for Cu<sub>4</sub>O<sub>3</sub> sample (a) nonimplanted, (b) implanted with Cr ions, SE model results after fitting for (c) CuO, (d) Cu<sub>4</sub>O<sub>3</sub>; thickness #1 represents interface between deposited layer and the substrate, thickness #2 is the main layer of thin films, thickness #3 with roughness are layers that represent influence of implantation.

CuO			Cu <sub>4</sub> O <sub>3</sub>		
Transition energies [eV]	T-L oscillator positions [eV]		Transition energies [eV]	T-L oscillator positions [eV]	
	non implanted	implanted		non implanted	implanted
1.66	0.84	1.08	1.80	0.52	0.38
2.07	2.40	2.16	2.34	1.96	1.92
2.68	3.28	3.29	3.08	2.87	2.70
3.46	6.09	5.70	3.53	3.37	3.26
			3.90	3.80	3.71
			5.29	3.84	3.75
			5.68	5.69	6.00

**Table 1.** Transition energies of CuO and Cu<sub>4</sub>O<sub>3</sub> from<sup>4</sup> and fitted Tauc–Lorentz oscillators position energies E<sub>0</sub>.

below. Therefore, to calculate the total thickness of the film, we need to add the thicknesses of three oxide layers and half of the roughness layer. The Cu<sub>4</sub>O<sub>3</sub> model is similar, the only difference being that the oxide layers consist of seven Tauc–Lorentz oscillators. Although in<sup>4</sup> five transitions are assigned to CuO, our model uses only four oscillators, because adding the fifth one did not improve the fitting. The resulting fitted thicknesses and the mean squared error obtained are presented in Fig. 3c,d. The roughness and top layer are the parts of the films that were influenced by implantation. The sum of their thicknesses (half of the roughness layer) increases with implantation, as the ions change the material properties in the depth of the sample. According to the SRIM simulation this depth is about 30 nm. The SE results show that the sum of layers R and #3 is about 30 nm for Cu<sub>4</sub>O<sub>3</sub>, 40 nm for CuO implanted with 15 keV energy ions.

The roughness layer is thicker for implanted samples than for nonimplanted samples in each case. The total thickness of the films is calculated as different than what was desired during the deposition process. It could be caused by nonidentical deposition conditions or limitations of the SE method which is an indirect one. The bottom layer's function in the model is to simulate the interface between the substrate and deposited oxide, therefore, the optical properties of this layer are not considered in the analysis of the optical properties of copper oxides. The layers in which we are interested are the top layer (#3) and the main layer (#2). In Fig. 4 the absorption coefficient, refractive index, and extinction coefficient of the studied samples are presented. In case of both oxides, the implantation reduced the absorption of material especially for energies higher than 3 eV. The optical parameters *n* and *k* also have lower values in most of the energy range after implantation.

In Fig. 4a we can see that CuO main layer absorption decreased and the energy band gap would increase. The slope of the absorption coefficient of the top layer is strongly reduced after implantation, which would indicate an increased Urbach energy and absorption by defects. For Cu<sub>4</sub>O<sub>3</sub>, we can observe this increase of Urbach energy more for the main layer (Fig. 4b). In the case of Cu<sub>4</sub>O<sub>3</sub>, the top layer is the source of more light absorption, both before and after implantation. The *n* and *k* characteristics show that the top layer has more profound oscillators in the fitted model. These two parameters also have higher values in the case of the top layer than in those for the main layer. Compared to the literature<sup>29</sup>, *n* and *k* are agreeable, the value *n* reaches a maximum of approximately 2.5–3 and decreases towards energies higher than 3 eV; *k* increases toward higher energies. The top layer has lowered its extinction coefficient after implantation to a greater extent than the main layer; this shows that the implantation process has a greater influence on the top of the sample. The absorption coefficient of CuO decreases after implantation, and the properties of the top layer changed more distinguishably than those of the main layer (Fig. 4a,c,e). The refractive index value falls from 2.5 to 1.5 with increasing energy (Fig. 4e), which is consistent with the literature<sup>30</sup>. Both *n* and *k* almost do not change for the main layer after implantation, while for the top layer their values decrease significantly, *n* from maximum 2.5–2.2, and *k* from maximum almost 1.2 to less than 0.8, and the maximum value of *k* shifts to higher energies. For both oxides, the drop in absorption originates mainly in decrease of amplitude of oscillators with energy positions of about 3.5 eV.

## Conclusions

In this work, we deposited thin films of CuO and Cu<sub>4</sub>O<sub>3</sub> that were subjected to implantation with Cr ions. Simulations of the implantation process allowed us to assess the range of sample depth in which implantation has a significant impact. XRD studies showed that samples with a thickness close to the ion penetration range were largely damaged, their crystallinity decreased, and phase changes occurred. The three-layer model based on Tauc–Lorentz oscillators gave a good fit with a mean squared error value less than 3. The determined values of the oscillator positions are close to the energy transition energies from the literature. The use of the three-layer model indicated that the change in the optical properties of the oxides came from a maximum layer depth of 45 nm, which is consistent with the results of the SRIM simulation. The calculated absorption coefficient is lower for implanted samples. Reducing the absorption of oxides is not a desirable effect for application as an absorber layer in a solar cell. Annealing and recrystallisation of the layers, leading to the distribution of the dopant throughout the volume of the layers, may result in a different effect, especially in the modification of the electrical properties of copper oxides. Thus, the next step of this research is to study thin films after annealing.

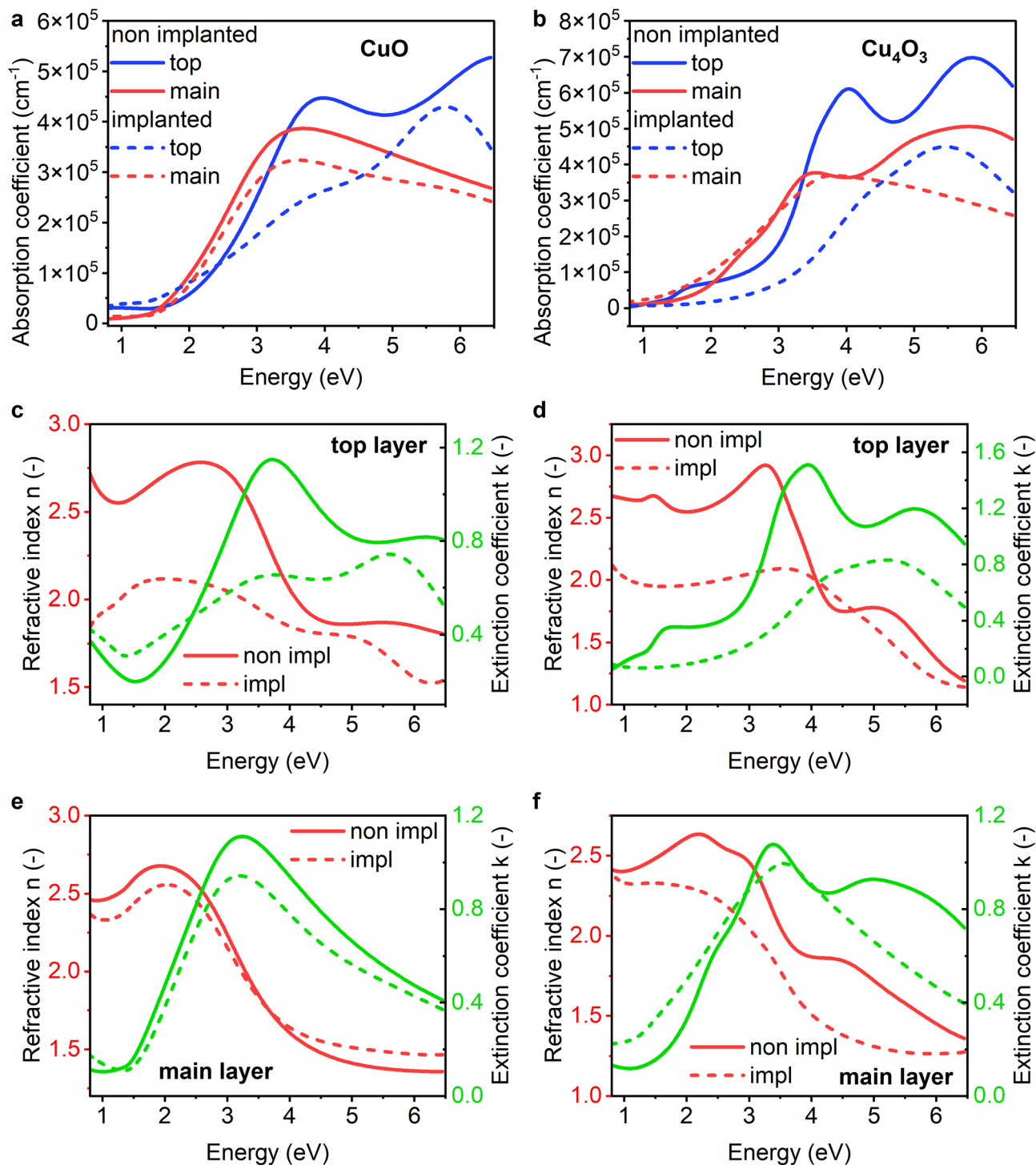


**Figure 4.** Optical properties of copper oxides: absorption coefficient of CuO top and main layers (a) and Cu<sub>4</sub>O<sub>3</sub> (b), refractive index and extinction coefficient of top layer of CuO (c) and Cu<sub>4</sub>O<sub>3</sub> (d), and for main layers of CuO (e) and Cu<sub>4</sub>O<sub>3</sub> (f).

#### Data availability

Data is available on request from the corresponding author.

Received: 15 October 2023; Accepted: 4 December 2023

Published online: 13 December 2023

## References

- Ribbing, C. G. & Roos, A. Copper Oxides (Cu<sub>2</sub>O, CuO) in *Handbook of Optical Constants of Solids* (ed. Palik, E. D.) 875–882. <https://doi.org/10.1016/B978-012544415-6.50085-6> (Academic Press, 1997).
- Reppin, D., Polity, A., Meyer, B. K. & Shokhovets, S. Optical and electrical properties of Cu<sub>2</sub>O, Cu<sub>4</sub>O<sub>3</sub> and CuO. *MRS Online Proc. Library* **1494**, 165–169. <https://doi.org/10.1557/opl.2012.1581> (2012).
- Pérez-Tomás, A., Mingorance, A., Tanenbaum, D. & Lira-Cantú, M. Metal oxides in photovoltaics: all-oxide, ferroic, and perovskite solar cells. In *The Future of Semiconductor Oxides in Next-Generation Solar Cells* 267–356. <https://doi.org/10.1016/B978-0-12-811165-9.00008-9> (Elsevier Inc., 2018).
- Meyer, B. K. *et al.* Binary copper oxide semiconductors: From materials towards devices. *Phys. Status Solidi B* **249**, 1487–1509. <https://doi.org/10.1002/pssb.201248128> (2012).
- Wong, T. K. S., Zhuk, S., Masudy-Panah, S. & Dalapati, G. K. Current status and future prospects of copper oxide heterojunction solar cells. *Materials* **9**, 271. <https://doi.org/10.3390/ma9040271> (2016).
- Rydosz, A., Dymal, K., Andrysiewicz, W., Grochala, D. & Marszałek, K. GLAD magnetron sputtered ultra-thin copper oxide films for gas-sensing application. *Coatings* **10**, 378. <https://doi.org/10.3390/coatings10040378> (2020).
- Andrysiewicz, W. *et al.* Flexible gas sensor printed on a polymer substrate for sub-ppm acetone detection. *Electron. Mater. Lett.* **16**, 146–155. <https://doi.org/10.1007/s13391-020-00199-z> (2020).
- Khiavi, N. D. *et al.* Visible light driven heterojunction photocatalyst of CuO-Cu<sub>2</sub>O thin films for photocatalytic degradation of organic pollutants. *Nanomaterials-Basel* **9**, 1011. <https://doi.org/10.3390/nano9071011> (2019).
- Kusior, A., Synowiec, M., Zakrzewska, K. & Radecka, M. Surface-controlled photocatalysis and chemical sensing of TiO<sub>2</sub>, α-Fe<sub>2</sub>O<sub>3</sub>, and Cu<sub>2</sub>O nanocrystals. *Crystals* **9**, 163. <https://doi.org/10.3390/cryst9030163> (2019).
- Kaphle, A., Echeverria, E., McLroy, D. N. & Hari, P. Enhancement in the performance of nanostructured CuO-ZnO solar cells by band alignment. *RSC Adv.* **10**, 7839–7854. <https://doi.org/10.1039/c9ra10771a> (2020).
- Minami, T., Nishi, Y. & Miyata, T. Efficiency enhancement using a Zn<sub>1-x</sub>Ge<sub>x</sub>O thin film as an n-type window layer in Cu<sub>2</sub>O-based heterojunction solar cells. *Appl. Phys. Express* **9**, 052301. <https://doi.org/10.7567/APEX.9.052301> (2016).
- Živković, A., Roldan, A. & de Leeuw, N. H. Density functional theory study explaining the underperformance of copper oxides as photovoltaic absorbers. *Phys. Rev. B* **99**, 035154. <https://doi.org/10.1103/PhysRevB.99.035154> (2019).
- Živković, A., Roldan, A. & De Leeuw, N. H. Tuning the electronic band gap of Cu<sub>2</sub>O via transition metal doping for improved photovoltaic applications. *Phys. Rev. Mater.* **3**, 115202. <https://doi.org/10.1103/PhysRevMaterials.3.115202> (2019).
- Minami, T., Nishi, Y. & Miyata, T. Heterojunction solar cell with 6% efficiency based on an n-type aluminum-gallium-oxide thin film and p-type sodium-doped Cu<sub>2</sub>O sheet. *Appl. Phys. Express* **8**, 022301. <https://doi.org/10.7567/APEX.8.022301> (2015).
- Nkhaili, L., Narjis, A., Outzourhit, A., El Kissani, A. & El Moznine, R. Investigation of the optical and electrical properties of ITO/ZnO/CdS/CuO:Co/Ag structure for solar cell. *Adv. Mater. Sci. Eng.* **2020**, 3907203. <https://doi.org/10.1155/2020/3907203> (2020).
- Rydosz, A. & Szkudlarek, A. Gas-sensing performance of M-doped CuO-based thin films working at different temperatures upon exposure to propane. *Sensors-Basel* **15**, 20069–20085. <https://doi.org/10.3390/s150820069> (2015).
- Nithya, S. *et al.* Ni doping in CuO: A highly sensitive electrode for sensing ammonia in ppm level using lanthanum gallate based electrolyte. *Mater. Res. Bull.* **118**, 110478. <https://doi.org/10.1016/j.materresbull.2019.05.003> (2019).
- Szkudlarek, A., Kollbek, K., Klejna, S. & Rydosz, A. Electronic sensitization of CuO thin films by Cr-doping for enhanced gas sensor response at low detection limit. *Mater. Res. Express* **5**, 126406. <https://doi.org/10.1088/2053-1591/aae0d8> (2018).
- Baturay, S., Candan, I. & Ozaydin, C. Structural, optical, and electrical characterizations of Cr-doped CuO thin films. *J. Mater. Sci. Mater. El.* **33**, 7275–7287. <https://doi.org/10.1007/s10854-022-07918-2> (2022).
- Kaur, M., Gautam, S. & Goyal, N. Ion-implantation and photovoltaics efficiency: A review. *Mater. Lett.* **309**, 131356. <https://doi.org/10.1016/j.matlet.2021.131356> (2022).
- Sealy, B. J. Ion implantation doping of semiconductors. *Int. Mater. Rev.* **33**, 38–52. <https://doi.org/10.1179/imr.1988.33.1.38> (1988).
- Bind, U. C. *et al.* Ion implantation induced phase transformation and enhanced crystallinity of as deposited copper oxide thin films by pulsed laser deposition. *Superlattice. Microst.* **84**, 24–35. <https://doi.org/10.1016/j.spmi.2015.03.064> (2015).
- Jafari, A. *et al.* Ion implantation of copper oxide thin films; statistical and experimental results. *Surf. Interfaces* **18**, 100463. <https://doi.org/10.1016/j.surf.2020.100463> (2020).
- Sisman, O. *et al.* Influence of iron and nitrogen ion beam exposure on the gas sensing properties of CuO nanowires. *Sensor. Actuat. B-Chem.* **321**, 128579. <https://doi.org/10.1016/j.snb.2020.128579> (2020).
- Shi, S., Gao, D., Xia, B. & Xue, D. Argon ion irradiation induced phase transition and room temperature ferromagnetism in the CuO thin film. *J. Phys. D Appl. Phys.* **49**, 055003. <https://doi.org/10.1088/0022-3727/49/5/055003> (2016).
- Yadav, R. *et al.* Defect-induced phase transformations in CuO thin films by Ag ion implantation and their gas-sensing applications. *J. Phys. Chem. C* **127**, 11438–11447. <https://doi.org/10.1021/acs.jpcc.3c01917> (2023).
- Ziegler, J. F., Ziegler, M. D. & Biersack, J. P. SRIM—The stopping and range of ions in matter. *Nucl. Instrum. Meth. B* **268**, 1818–1823. <https://doi.org/10.1016/J.NIMB.2010.02.091> (2010).
- Ungeheuer, K. *et al.* Influence of Cr ion implantation on physical properties of CuO thin films. *Int. J. Mol. Sci.* **23**, 4541. <https://doi.org/10.3390/IJMS23094541> (2022).
- Pierson, J. F., Duverger, E. & Banakh, O. Experimental and theoretical contributions to the determination of optical properties of synthetic paramelaconite. *J. Solid State Chem.* **180**, 968–973. <https://doi.org/10.1016/j.jssc.2006.12.028> (2007).
- Ito, T., Yamaguchi, H., Masumi, T. & Adachi, S. Optical properties of CuO studied by spectroscopic ellipsometry. *J. Phys. Soc. Jpn.* **67**, 3304–3309. <https://doi.org/10.1143/JPSJ.67.3304> (1998).

## Acknowledgements

Research project supported by program “Excellence initiative—research university” for the AGH University of Science and Technology, project no. 4121. We wish to thank PhD M. Perzanowski for XRD measurements and PhD K. Dymal for help with ellipsometry modelling.

## Author contributions

Conceptualization—K.U., K.W.M.; data curation—K.U.; formal analysis—K.U.; funding acquisition—K.W.M.; investigation—K.U.; methodology—K.U., M.M.-N., A.R.; project administration—K.U., K.W.M.; resources—M.M.-N., A.R., K.U., K.W.M.; software—K.U.; supervision—K.W.M.; validation—K.U., Visualization—K.U.; writing—original draft—K.U.; writing—review and editing—K.U., K.W.M.

## Competing interests

The authors declare no competing interests.



### Additional information

**Correspondence** and requests for materials should be addressed to K.U.

**Reprints and permissions information** is available at [www.nature.com/reprints](http://www.nature.com/reprints).

**Publisher's note** Springer Nature remains neutral with regard to jurisdictional claims in published maps and institutional affiliations.



**Open Access** This article is licensed under a Creative Commons Attribution 4.0 International License, which permits use, sharing, adaptation, distribution and reproduction in any medium or format, as long as you give appropriate credit to the original author(s) and the source, provide a link to the Creative Commons licence, and indicate if changes were made. The images or other third party material in this article are included in the article's Creative Commons licence, unless indicated otherwise in a credit line to the material. If material is not included in the article's Creative Commons licence and your intended use is not permitted by statutory regulation or exceeds the permitted use, you will need to obtain permission directly from the copyright holder. To view a copy of this licence, visit <http://creativecommons.org/licenses/by/4.0/>.

© The Author(s) 2023